GEOPHYSICS, VOL. 82, NO. 6 (NOVEMBER-DECEMBER 2017); P. Q67–Q78, 17 FIGS.
10.1190/GEO2016-0560.1

A new approach to separate seismic time-lapse time shifts in the reservoir and overburden

Yi Liu[1], Martin Landrø[1], Børge Arntsen[1], Joost van der Neut[2], and Kees Wapenaar[2]

ABSTRACT

For a robust way of estimating time shifts near horizontal boreholes, we have developed a method for separating the reflection responses above and below a horizontal borehole. Together with the surface reflection data, the method uses the direct arrivals from borehole data in the Marchenko method. The first step is to retrieve the focusing functions and the up-down wavefields at the borehole level using an iterative Marchenko scheme. The second step is to solve two linear equations using a least-squares minimizing method for the two desired reflection responses. Then, the time shifts that are directly linked to the changes on either side of the borehole are calculated using a standard crosscorrelation technique. The method is applied with good results to synthetic 2D pressure data from the North Sea. One example uses purely artificial velocity changes (negative above the borehole and positive below), and the other example uses more realistic changes based on well logs. In the 2D case with an adequate survey coverage at the surface, the method is completely data driven. In the 3D case in which there is a limited number of horizontal wells, a kinematic correct velocity model is needed, but only for the volume between the surface and the borehole. Possible error factors related to the Marchenko scheme, such as an inaccurate source wavelet, imperfect surface multiples removal, and medium with loss are not included in this study.

INTRODUCTION

Seismic time-lapse analysis has become a standard tool for subsurface monitoring in the petroleum industry. By studying the difference in the data from repeated seismic surveys, useful information from the field can be obtained, such as velocity, pressure, and saturation changes. One of the first commercial successes of time-lapse seismic in the North Sea is the Gullfaks study (Landrø et al., 1999), in which the evident effect of replacing oil with water in the seismic data helps with the successful identification of remaining and untouched oil pockets.

The changes between the repeated surveys can be explored in many ways. One common technique is to find and analyze the time shift, and this is the main subject of this paper. Other methods, such as waveform inversion that takes into account the traveltime and the amplitude to estimate changes of elastic properties, are also used (Raknes and Arntsen, 2014; Maharramov et al., 2015, 2016). Some issues related to survey repeatability can be addressed with those methods. Here, we focus on the traveltime shift estimations because they remain a main tool for time-lapse studies and can be linked to physical strain and velocity changes (Landrø and Stammeijer, 2004), for example, reservoir compaction (Røste et al., 2015). Barkved and Kristiansen (2005) show a field example of how compaction in a reservoir can be observed in time-lapse seismic data. Røste et al. (2007) use the observed time shifts in prestack ocean bottom cable data to discriminate layer thickness and velocity changes. For anisotropic media, Fuck et al. (2009) give an analytical description of stress-related traveltime shifts and show that anisotropy parameters can be estimated based on the offset dependence of the time shifts.

Surface reflection data (Meunier and Huguet, 1998) and borehole data (Meunier et al., 2001; Guilbot and Smith, 2002) are used for time-lapse studies. To calculate the time shifts, the standard procedure is done by crosscorrelation (Hatchell and Bourne, 2005). Other more advanced methods such as nonlinear inversion (Rickett et al., 2007) and the correlated leakage method have also been proposed and comparisons are made (Whitcombe et al., 2010). However because traveltime changes are cumulative along the raypaths

Manuscript received by the Editor 1 November 2016; revised manuscript received 2 June 2017; published ahead of production 19 July 2017; published online 29 August 2017.
[1]Norwegian University of Science and Technology, Department of Geoscience and Petroleum, Trondheim, Norway. E-mail: yi.liu@ntnu.no; martin.landro@ntnu.no; borge.arntsen@ntnu.no.
[2]Delft University of Technology, Department of Geoscience and Engineering, Delft, The Netherlands. E-mail: j.r.vanderneut@tudelft.nl; c.p.a.wapenaar@tudelft.nl.

and the sources are usually placed close to the surface, the changes in the deep area cannot be directly linked to the observed time shifts. In addition, strong multiple reflections in the data may hinder the event picking, eventually making the time shift estimation difficult, especially for deep sections.

For the problem of the accumulative traveltime, the use of a fractional change of time shift (also called time strain) (Rickett et al., 2007) has been proposed, but one disadvantage is that the differentiation tends to boost noise. An example of using time strain for estimation of reservoir pressure changes is shown by Hodgson et al. (2007). On the other hand, methods related to seismic interferometry (Snieder et al., 2009; Wapenaar et al., 2011; Galetti and Curtis, 2012) can be used to virtually move surface sources below a complex overburden and therefore enable time-lapse monitoring of reservoir without any velocities of the overburden (Bakulin and Calvert, 2006). Mehta et al. (2008) improve the method using multicomponent data to remove the spurious events related to the reflections in the overburden from retrieved responses.

For the attenuation of internal multiples, a classic approach is building a multiple model and adaptively subtracting it from the data by computing shaping filters (Guitton and Verschuur, 2004). Another approach is using multicomponent data for up-down separation (Amundsen, 2001). Given single-component data and a smooth background velocity model, a new focusing method that goes beyond interferometry, called the Marchenko method (Broggini et al., 2012; Wapenaar et al., 2013, 2016; Behura et al., 2014), meets the requirement of effectively removing internal multiples. The method enables one to create virtual sources at any position inside a medium, but a macrovelocity model that describes the kinematics of the wavefield is nevertheless necessary. Examples of its application for internal multiple removal are shown by Meles et al. (2015) and Ravasi et al. (2016). However, velocity errors in the model affect the method to various degrees (Thorbecke et al., 2013; de Ridder et al., 2016). For the method's application for robust imaging near horizontal boreholes, Liu et al. (2016) propose the combination of surface reflection data and horizontal borehole data to replace the dependency on a background velocity model. Two separate reflection responses can be obtained, one for the overburden and one for the underburden (the area below a horizontal borehole, including the reservoir). All internal multiples from the other side of the borehole are removed, and imaging with good positioning of the reflectors near the borehole can be obtained with crude velocities.

In this paper, we show that it is possible to address both of the above problems by combining the surface and borehole data. By repeating two of the proposed schemes in Liu et al. (2016) on the base and monitor data, the time shifts in the overburden and the underburden can be separated and subtle time shifts near the horizontal borehole can be estimated without any event picking on the data. Then, standard time shift analysis can be performed for each side of the borehole independently. This offers the same benefits as Bakulin and Calvert (2006), but it also addresses changes above the borehole. In addition, internal multiples can be taken into account without using multicomponent data, and a velocity model is not needed.

We first explain the preprocessing sequence, followed by the numerical demonstration based on two field velocity models. A velocity change that is purely negative in the overburden and positive in the underburden is used in the first example. A more realistic velocity change model based on the Gullfaks field is used in the second example, and the results are compared with field observations. Then, we discuss the benefits and limitations of the method.

METHOD

In this section, besides the conventional surface seismic data geometry, we assume that the borehole data are available at a constant depth (e.g., from a horizontal well) with sources at the surface. The word "underburden" is used to refer to the medium that is below the borehole (including the reservoir). Although the method is presented with a configuration of a horizontal borehole, the application can be extended to deviated wells, and this will be discussed in a later section. Free-surface multiple removal and source signal deconvolution are assumed in the surface reflection data. The data are denoted as measured band-limited Green's functions in the equations.

The aim of the preprocessing is to use a data-driven method to reconstruct the reflection responses of the overburden and the underburden, individually, at a constant (borehole) level. The notation convention used throughout the paper is that a spatial position is denoted by $\mathbf{x} = (x_1, x_2, x_3)$, with $x_3 = 0$ at the surface, ∂D_0, and x_3 is increasing positively downward. Coordinates at any boundary, e.g., at the depth level ∂D_i (which indicates the horizontal borehole depth level in this paper), are denoted as $\mathbf{x}_i = (\mathbf{x}_H, x_{3,i})$, with $\mathbf{x}_H = (x_1, x_2)$. Position $\mathbf{x}_i'$ represents a focusing position at a lateral coordinate $\mathbf{x}_H'$ at the depth level ∂D_i, and $\mathbf{x}_0''$ represents a position at lateral coordinate $\mathbf{x}_H''$ at the surface level ∂D_0. This notation convention is summarized in Figure 1. In Figure 1, the two blue solid lines show examples of the raypaths of the two unknown reflection responses to be solved.

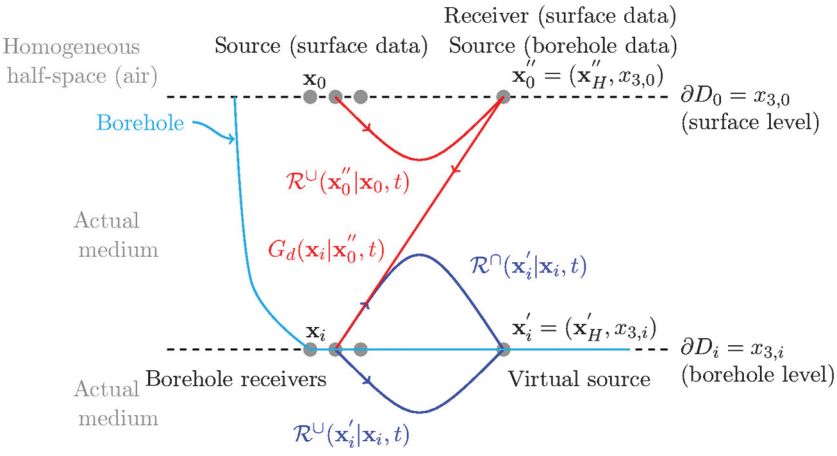

Figure 1. Notation convention and coordinate definition. Each spatial position is denoted by $(\mathbf{x}_H, x_{3,i})$, with $\mathbf{x}_H = (x_1, x_2)$ and i represents a certain depth level. Here, ∂D_0 denotes a transparent surface level, above which the medium is homogeneous, and ∂D_i denotes a horizontal borehole level. The blue solid lines represent the unknown reflection responses, where $\mathcal{R}^{\cup}(\mathbf{x}_i'|\mathbf{x}_i, t)$ contains only reflections coming from below the borehole and $\mathcal{R}^{\cap}(\mathbf{x}_i'|\mathbf{x}_i, t)$ contains only reflections coming from above the borehole. These two responses are the unknown responses to be solved. The red solid line represents the known surface reflection response.

The reflection response $\mathcal{R}^{\cap}(\mathbf{x}_i'|\mathbf{x}_i,t)$ is the response of the overburden and contains no interaction with the part of the medium below the borehole, whereas $\mathcal{R}^{\cup}(\mathbf{x}_i'|\mathbf{x}_i,t)$ is that of the underburden and contains no interaction with the part of the medium above the borehole. The surface reflection response $\mathcal{R}^{\cup}(\mathbf{x}_0''|\mathbf{x}_0,t)$ is known from the surface data, indicated by the red solid line in Figure 1. The bold-faced variables indicate vectors.

Reconstruction of the reflection responses

The two unknown reflection responses (the blue quantities in Figure 1) can be found by solving the following two equations in the frequency domain (Wapenaar et al., 2014):

$$\hat{f}_2^{+}(\mathbf{x}_i'|\mathbf{x}_0'') = \int_{\partial D_i} \hat{\mathcal{R}}^{\cap}(\mathbf{x}_i'|\mathbf{x}_i)\hat{f}_2^{-}(\mathbf{x}_i|\mathbf{x}_0'')d\mathbf{x}_i; \tag{1}$$

$$\hat{G}^{-}(\mathbf{x}_i'|\mathbf{x}_0'') = \int_{\partial D_i} \hat{\mathcal{R}}^{\cup}(\mathbf{x}_i'|\mathbf{x}_i)\hat{G}^{+}(\mathbf{x}_i|\mathbf{x}_0'')d\mathbf{x}_i. \tag{2}$$

The symbol $\hat{}$ above the quantities denotes the frequency domain. Here, the first equation relates the unknown reflection response of the overburden $\hat{\mathcal{R}}^{\cap}(\mathbf{x}_i'|\mathbf{x}_i)$ to pressure-normalized one-way focusing functions $\hat{f}_2^{\pm}(\mathbf{x}_i'|\mathbf{x}_0'')$, and the second equation relates the unknown reflection response of the underburden $\hat{\mathcal{R}}^{\cup}(\mathbf{x}_i'|\mathbf{x}_i)$ to the upgoing and downgoing wavefields ($\hat{G}^{-}(\mathbf{x}_i'|\mathbf{x}_0'')$ and $\hat{G}^{+}(\mathbf{x}_i'|\mathbf{x}_0'')$) at $\mathbf{x}_i'$ from a surface source at $\mathbf{x}_0''$.

A central element in the Marchenko method is formed by the focusing functions, and there are two types of them, $f_1^{\pm}(\mathbf{x}_0''|\mathbf{x}_i',t)$ and $f_2^{\pm}(\mathbf{x}_i'|\mathbf{x}_0'',t)$. Because details can be found in many previous publications, we skip a complete introduction on this. Briefly speaking, the focusing functions satisfy the 3D wave equation with specific boundary conditions, and they are mutually related via

$$f_1^{+}(\mathbf{x}_0''|\mathbf{x}_i',t) = f_2^{-}(\mathbf{x}_i'|\mathbf{x}_0'',t); \tag{3}$$

$$-f_1^{-}(\mathbf{x}_0''|\mathbf{x}_i',-t) = f_2^{+}(\mathbf{x}_i'|\mathbf{x}_0'',t). \tag{4}$$

By using these mutual relations, equation 1 can be expressed using only $\hat{f}_1^{\pm}(\mathbf{x}_0''|\mathbf{x}_i')$. But to keep the clarity that the left side of equation 1 is a downgoing wave, both focusing functions are kept in this paper. All necessary quantities needed to solve equations 1 and 2 can be found by computing the focusing function $f_1^{\pm}(\mathbf{x}_0''|\mathbf{x}_i',t)$.

Here, we use an iterative Marchenko scheme (Wapenaar et al., 2013) to find $f_1^{+}(\mathbf{x}_0''|\mathbf{x}_i',t)$ and $f_1^{-}(\mathbf{x}_0''|\mathbf{x}_i',t)$ using the reflection response measured at the surface ∂D_0 and the direct wavefield measured in the borehole. The iterative scheme reads,

$$f_{1,k}^{+}(\mathbf{x}_0''|\mathbf{x}_i',t) = f_{1,0}^{+}(\mathbf{x}_0''|\mathbf{x}_i',t) + \theta(t + t_d(\mathbf{x}_0''|\mathbf{x}_i')) \int_{\partial D_0}\int_{-\infty}^{\infty} \mathcal{R}^{\cup}(\mathbf{x}_0''|\mathbf{x}_0',t')f_{1,k-1}^{-}(\mathbf{x}_0'|\mathbf{x}_i',t+t')dt'd\mathbf{x}_0', \tag{5}$$

$$f_{1,k}^{-}(\mathbf{x}_0''|\mathbf{x}_i',t) = \theta(t_d(\mathbf{x}_0''|\mathbf{x}_i') - t) \int_{\partial D_0}\int_{-\infty}^{\infty} \mathcal{R}^{\cup}(\mathbf{x}_0''|\mathbf{x}_0',t-t')f_{1,k}^{+}(\mathbf{x}_0'|\mathbf{x}_i',t')dt'd\mathbf{x}_0', \tag{6}$$

with

$$f_{1,0}^{+}(\mathbf{x}_0''|\mathbf{x}_i',t) \approx G_d(\mathbf{x}_i'|\mathbf{x}_0'',-t), \tag{7}$$

where $\theta(t)$ is the Heaviside function that passes the results for $t > 0$. The subscript zero indicates the initial estimate, which is approximated by the time-reversed direct wavefield $G_d(\mathbf{x}_i'|\mathbf{x}_0'',-t)$ measured in the borehole. This is more accurate than to obtain $G_d(\mathbf{x}_i'|\mathbf{x}_0'',-t)$ from a velocity model. As it is actually measured, subtle time shifts in the overburden are taken into account, even if they are not known. The notation here is changed to the time domain due to the time window function used. For our application, this "direct first" assumption is satisfied because the receiver spacing in the borehole data is not large and the medium varies smoothly. To extract the direct wavefield, a time gate can be used for small offsets. For large offsets, the direct arrivals intersect the refracted events, dip filtering, or the picking of the traveltime curve with the maximum amplitudes can be used. Then, together with the input of the surface reflection response $\mathcal{R}^{\cup}(\mathbf{x}_0''|\mathbf{x}_0,t)$ and the traveltime $t_d(\mathbf{x}_i'|\mathbf{x}_0'')$ (from the borehole data), $f_1^{\pm}(\mathbf{x}_0|\mathbf{x}_i',t)$ can be computed without any velocity information.

Now with $f_1^{\pm}(\mathbf{x}_0|\mathbf{x}_i',t)$ known, so are the upgoing and downgoing parts of $f_2(\mathbf{x}_i'|\mathbf{x}_0,t)$ by the mutual relation in equations 3 and 4. Then, the reflection response of the overburden $\hat{\mathcal{R}}^{\cap}(\mathbf{x}_i'|\mathbf{x}_i)$ in equation 1 can be solved for each frequency using, for instance, a standard damped least-squares approach (Menke, 1989). To solve for the reflection response of the underburden $\hat{\mathcal{R}}^{\cup}(\mathbf{x}_i'|\mathbf{x}_i)$ in equation 2, an extra step of computing the upgoing and downgoing wavefields ($G^{-}(\mathbf{x}_i'|\mathbf{x}_0'',t)$ and $G^{+}(\mathbf{x}_i'|\mathbf{x}_0'',t)$, respectively) is needed. They are related to the focusing function and the surface reflection response via the following equations (Wapenaar et al., 2014), as long as $t \geq t_d(\mathbf{x}_i'|\mathbf{x}_0'')$:

$$G^{-}(\mathbf{x}_i'|\mathbf{x}_0'',t) = \int_{\partial D_0}\int_{-\infty}^{t} \mathcal{R}^{\cup}(\mathbf{x}_0''|\mathbf{x}_0,t-t') f_1^{+}(\mathbf{x}_0|\mathbf{x}_i',t')dt'd\mathbf{x}_0 \tag{8}$$

and

$$G^{+}(\mathbf{x}_i'|\mathbf{x}_0'',t) = f_{1,0}^{+}(\mathbf{x}_0''|\mathbf{x}_i',-t) - \int_{\partial D_0}\int_{-\infty}^{t} \mathcal{R}^{\cup}(\mathbf{x}_0''|\mathbf{x}_0,t-t') f_1^{-}(\mathbf{x}_0|\mathbf{x}_i',-t')dt'd\mathbf{x}_0, \tag{9}$$

where $\mathcal{R}^{\cup}(\mathbf{x}_0''|\mathbf{x}_0,t)$ (the surface reflection response), $f_1^{\pm}(\mathbf{x}_0|\mathbf{x}_i',t)$ (the one-way focusing functions), and $t_d(\mathbf{x}_i'|\mathbf{x}_0'')$ (the direct arrival's traveltime in the borehole data) are already known. After this step, $\hat{\mathcal{R}}^{\cup}(\mathbf{x}_i'|\mathbf{x}_i)$ can be solved for in equation 2 in a similar manner as in equation 1.

The overall workflow is summarized in Figure 2. This workflow is repeated for the base and monitor data, and it results in two new separate data sets for time shift estimation: one for the underburden and one for the overburden.

Our understanding of the method might also be helped by Figure 3. The red quantities in Figure 3a indicate the input surface reflection response and the direct wavefield measured in the borehole. The method aims to find the blue quantities in Figure 3b and 3c. These new reflection responses are particularly useful for time-lapse traveltime analysis of the area near the borehole, complementing

that from the original surface and borehole data. The sources and the receivers in these virtual responses are virtually moved to the borehole position, so the traveltime accumulates away from the borehole level. Because the distance to the target is shorter, the observed time shifts can be more directly related to changes in the vicinity of the borehole without any prior information of the shallower section. Furthermore, there are no reflections coming from the other side of the borehole, improving the overall signal-to-noise ratio (S/N).

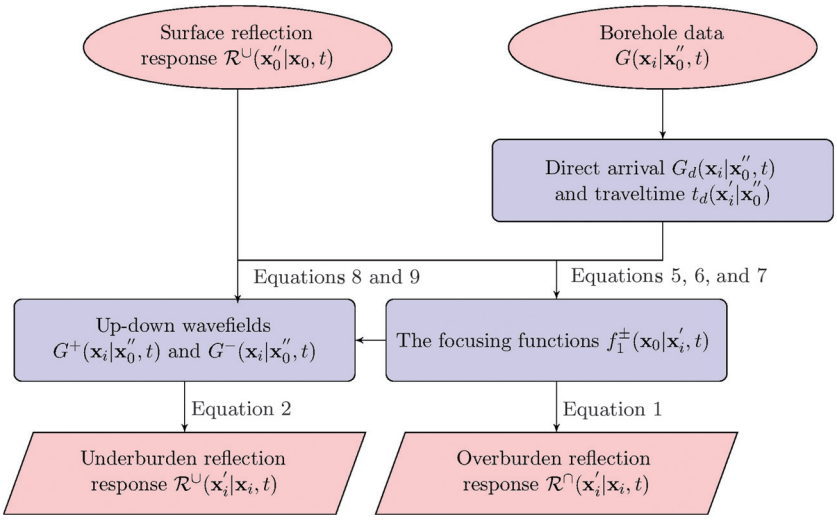

Figure 2. Flowchart illustration of the method. The ellipses denote the input, and the trapezia denote the output. The intermediate steps are marked with boxes.

Time shift estimation

To estimate the time shift, a standard crosscorrelation technique is used in this paper. No event picking is performed prior to the crosscorrelation to show that accurate time shift characterization near the borehole can be achieved automatically with this approach.

Depending on the magnitude of the time shift, it might be necessary to interpolate the new responses to a smaller time interval first, and a suitable time window is used for crosscorrelation. A certain minimum threshold value is chosen based on the crosscorrelation amplitude value for picking the time lag. Repeating the crosscorrelation for all receiver positions gives the overall time shift maps. The time strain maps

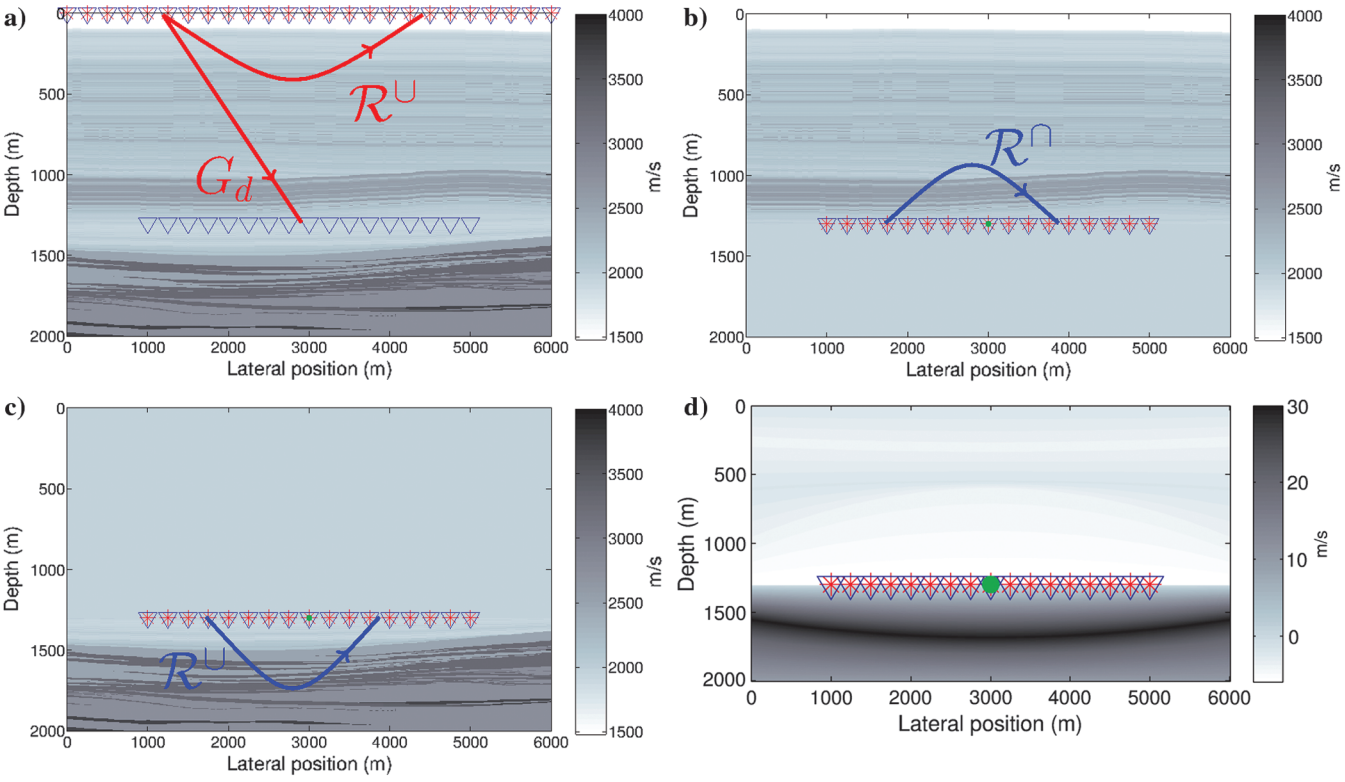

Figure 3. P-wave velocity model and data set geometries. The stars denote sources, and the triangles denote receivers. The red letters denote the input data, and the blue letters denote the unknown responses. (a) The base velocity model. The configuration shows two survey geometries. The surface data have sources and receivers at the surface level, and the borehole data have sources at the surface and receivers in the borehole. (b) The medium configuration in which the responses of the overburden are constructed. The sources are virtually moved to the borehole level, and because the underburden is homogeneous, there are no upgoing reflections in the new responses. (c) The same as (b) but for the underburden. (d) The velocity change. The changes are artificial for the testing purpose. There is a velocity increase of up to 30 m/s below the borehole and a velocity decrease of up to 6 m/s above the borehole, such that positive time shifts (monitor-base) should be observed for the overburden and negative time shifts for the underburden. The green circle shows one reference new source location.

can be calculated by taking the fractional difference of the time shift. The calculated time shift and the time strain maps of the overburden and the underburden are independent of each other, and more analysis linking the result to the geomechanical changes follows.

NUMERICAL EXAMPLES

Vankeulen model

The first example is based on the Vankeulen field in the North Sea, which is shown in Figure 3a. For the surface data, there are 241 sources and receivers at the free surface. For the borehole data, there are 241 sources at the free surface and 161 receivers at a depth of 1300 m. The source and receiver spacings are 25 m. The source signal in the borehole data is a Ricker wavelet with a peak frequency of 15 Hz, and that in the surface data has a flat spectrum up to 48 Hz. A finite-difference method (Thorbecke and Draganov, 2011) is used for modeling, and the surface related multiples are not included. For the monitor model, artificial velocity changes are made (Figure 3d), in which there is a maximum velocity increase of 30 m/s below the borehole and a maximum velocity decrease of 6 m/s occurs above the borehole. With these velocity changes, it is expected to observe only positive time shifts in the overburden and only negative time shifts in the underburden from the new responses.

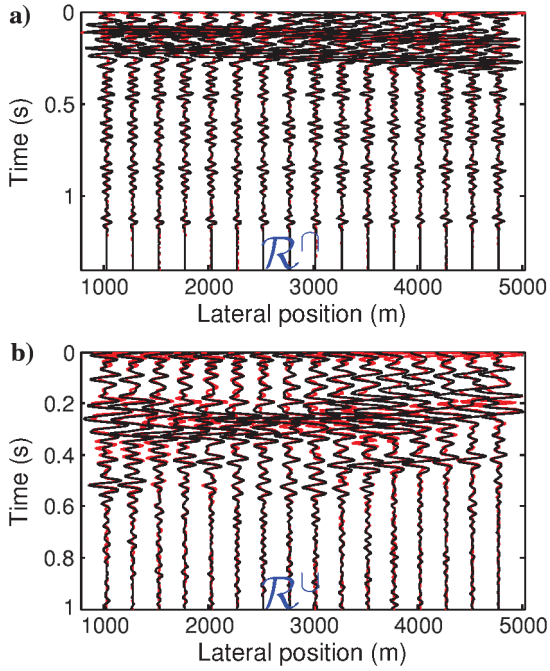

Figure 4. The zero-offset trace comparison with the modeled reference traces. The new response is in red and the reference is in black. In these new responses, the sources are virtually moved to the borehole level and the receiver positions are the same as in the original borehole survey, as shown in Figure 3b and 3c. The direct arrivals are removed, and the trace amplitude is normalized. The reflection response of (a) the overburden and (b) the underburden. It shows that reflections from each side of the borehole are separated, including the internal multiples. The mismatch at the beginning of the traces in (a) is most likely due to the reflectors very close to the borehole.

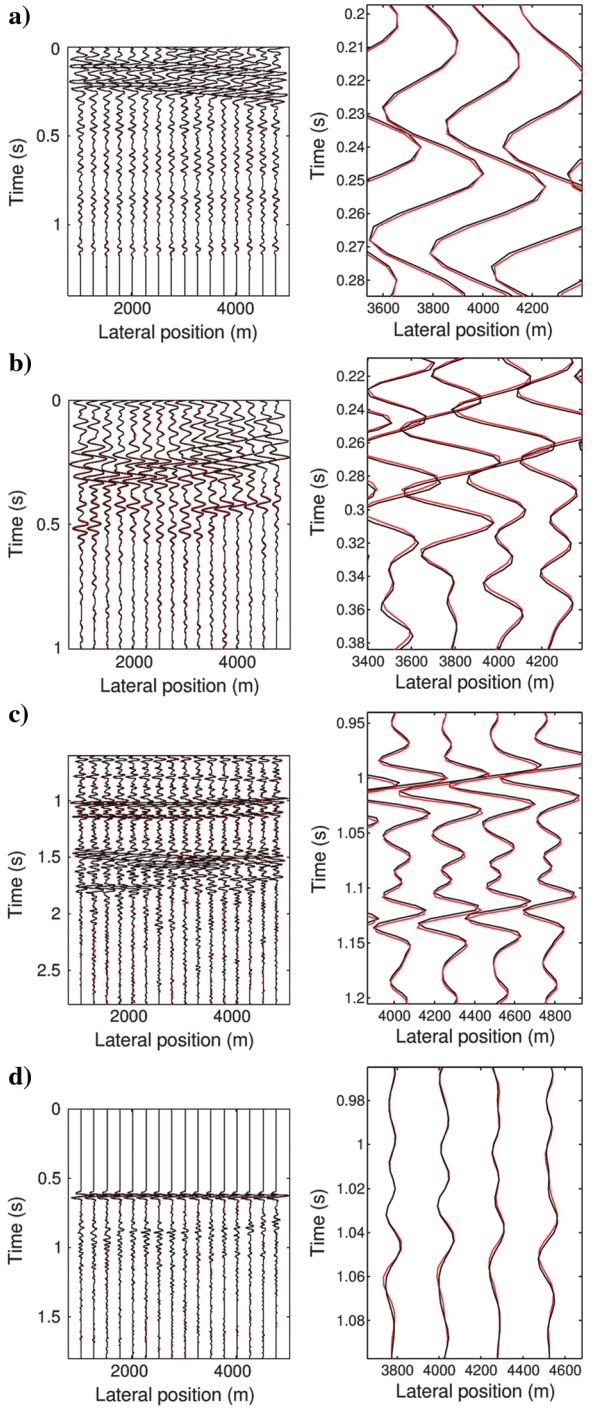

Figure 5. The overall zero-offset trace view of the base response (in black) and monitor data (in red). A magnified view is shown on the right in each panel. The new response of (a) the overburden and (b) the underburden. It is observed in (b) that the monitor response has a smaller traveltime than the base response, indicating a velocity increase. The original response from (c) the surface data (with the direct arrivals removed) and (d) the borehole data, in which the direct arrivals are kept because they contain information of the changes in the overburden. In the magnified windows, only the increase of traveltime is observed in both original data sets, unlike in the new response in (b). Besides, the ambiguity of the primary reflections and the internal multiples are also problematic for time shift estimation near the borehole in (c and d).

The goal is to transform the original data sets into what would be recorded as if they were modeled in the two reference states as shown in Figure 3b and 3c, so that the different time shifts caused by the changes in the overburden and the underburden are separated. In these two reference states, the source and receivers are moved to the borehole depth. Furthermore, the velocity on the other side of the borehole is homogenized, meaning that the interfering reflections from the other side are removed in the new responses. This leads to a higher S/N ratio compared with the original data.

Applying the process flow (Figure 2) to the base and monitor data, the new reflection responses of the overburden and the underburden are retrieved. For validation, the zero-offset gathers are checked against the directly modeled traces in Figure 4. These reference traces are modeled according to Figure 3b and 3c, and the direct arrivals are removed. The trace amplitudes are normalized in the figure. This comparison validates the correct retrieval of our new responses. The figure shows that the phases of the reflections match well, even for the later arrivals, meaning that the multiples from the other side are indeed removed.

Next, for an overview of the new responses, all zero-offset monitor traces are plotted in red against the base traces in black in Figure 5. In the magnified insets in Figure 5b (the new response of the underburden), the shorter traveltime in the red monitor traces can be noticed, whereas this shorted traveltime is not directly observable in Figure 5c (the original surface response) and Figure 5d (the original borehole response). In addition, the clear separation of the reflections on each side of the borehole is appreciated in the new response from Figure 5a and 5b, compared with Figure 5c and 5d.

To check the new time shifts, Figure 6 shows the detailed result for the lateral position of 3025 m, in which a standard crosscorrelation method (Landrø et al., 2001) is used. All zero-offset traces are first interpolated to a sampling interval of 0.4 ms, and then a sliding crosscorrelation window 0.2 s is used. Figure 6a and 6c shows the velocity change (monitor-base) profiles along $x_1 = 3025$ m in the overburden and the underburden, respectively. Figure 6b and 6d shows the time shifts from the new response in blue, checked against those from the modeled response in red (dashed-dotted line) and those directly obtained from the velocities in green (dashed line). The comparison confirms that the new time shifts agree well with the given velocity model and that small time shifts from the deep part of the model can be found with this data-driven approach.

Figures 7 and 8 show the overall time shift maps and the time strain maps, respectively. Figure 7a joins the time shift maps of the overburden and the underburden, and the dashed line denotes the borehole depth. Each half is calculated independently from the new responses. It clearly shows that the opposite time shifts are separated by this method. For comparison, the time shift maps from the original surface and borehole data are shown in Figure 7b and 7c, respectively. We see that a big difference between the new map in

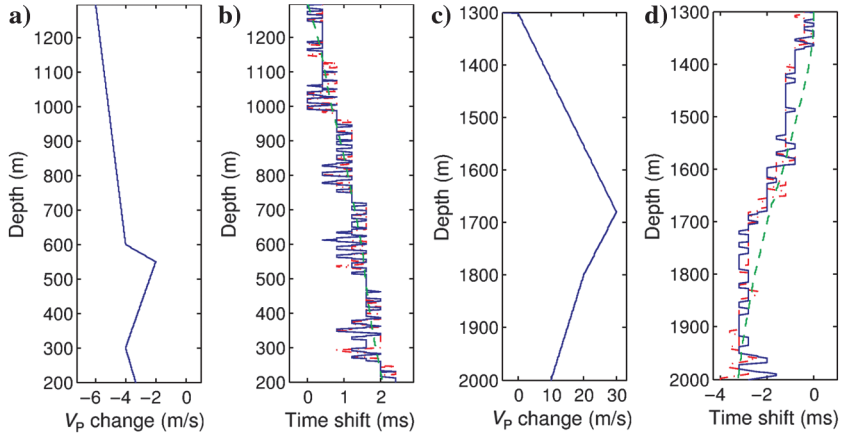

Figure 6. The velocity change profiles at $x_1 = 3025$ m of (a) the overburden and (c) the underburden. (b and d) The estimated time shifts from the new responses in Figure 5a and 5b, respectively. The blue line is obtained from the retrieved new response using crosscorrelation, and the red dashed-dotted line is obtained from the modeled reference response. The green dashed line is obtained by directly computing the time shifts from the velocities. The crosscorrelation window size is 0.2 ms. The vertical axis in (a) is flipped to reflect that the retrieved response here is obtained from below (as in Figure 3b). For a direct comparison, the time shifts by crosscorrelation are converted to depth using the base velocities. It is observed that the different time shifts in the overburden and the underburden are well-separated, and the new estimate in blue agrees well with those in red and green.

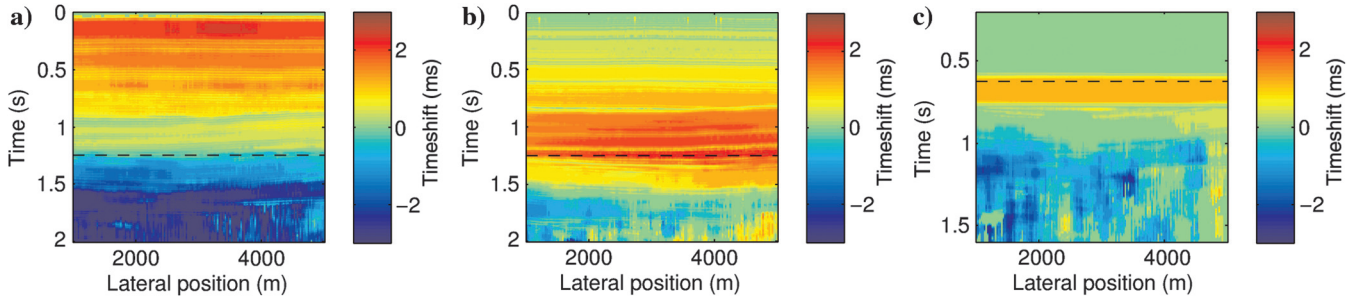

Figure 7. The smoothed time shift maps. (a) The joined map of the overburden and the underburden, calculated separately using the new responses. (b and c) The maps from the original surface reflection and the borehole data, respectively. The dashed line indicates the borehole depth in time, which is the two-way traveltime in (a and b), and the one-way traveltime in (c). The crosscorrelation window is 0.2 s for all panels. The new joined map in (a) shows the separated positive and negative time shifts clearly, whereas the accumulative nature of traveltime for deep events needs to be taken into account when interpreting the results in (b and c).

Figure 7a and the map in Figure 7b is that the time shift accumulates from different depths. One from the borehole depth, and the other from the surface. Therefore, for studying the medium changes near borehole, this new approach has its advantage. It can also be observed that in the time strain maps (Figure 8), more details of the reflectors below the borehole are shown by the new approach (Figure 8a) than the maps from the surface data (Figure 8b) and the borehole data (Figure 8c).

Gullfaks model

The second example is based on the Gullfaks field, where the time-lapse seismic method has been applied with great success. Different from the previous example, here the velocity changes are made more realistic according to the geologic structures and field measurements. We first present the result, then we make comparison with the field observation in a separate subsection.

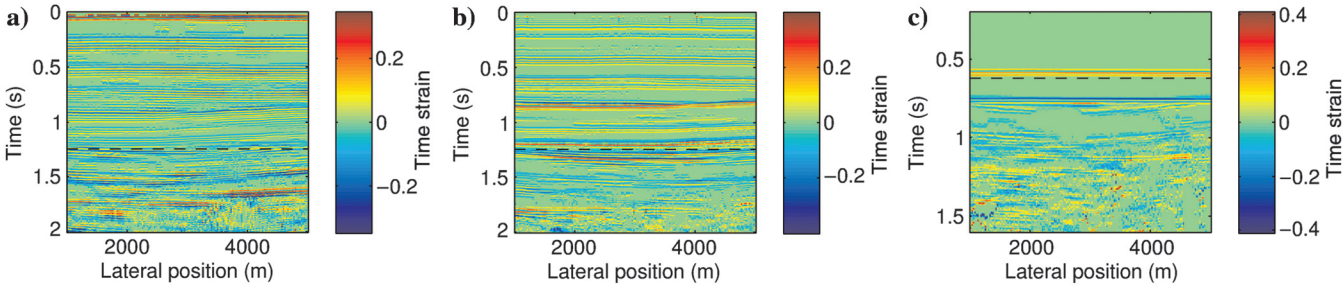

Figure 8. The time strain maps based on Figure 7. (a) The joined map of the overburden and the underburden. (b and c) The maps from the original the surface reflection and the borehole data, respectively. The dashed line indicates the borehole depth in time. More details of the underburden are noticeable in (a) than in (c) or (d), and they agree well with the geologic model (Figure 3a) and the synthetic velocity change (Figure 3d).

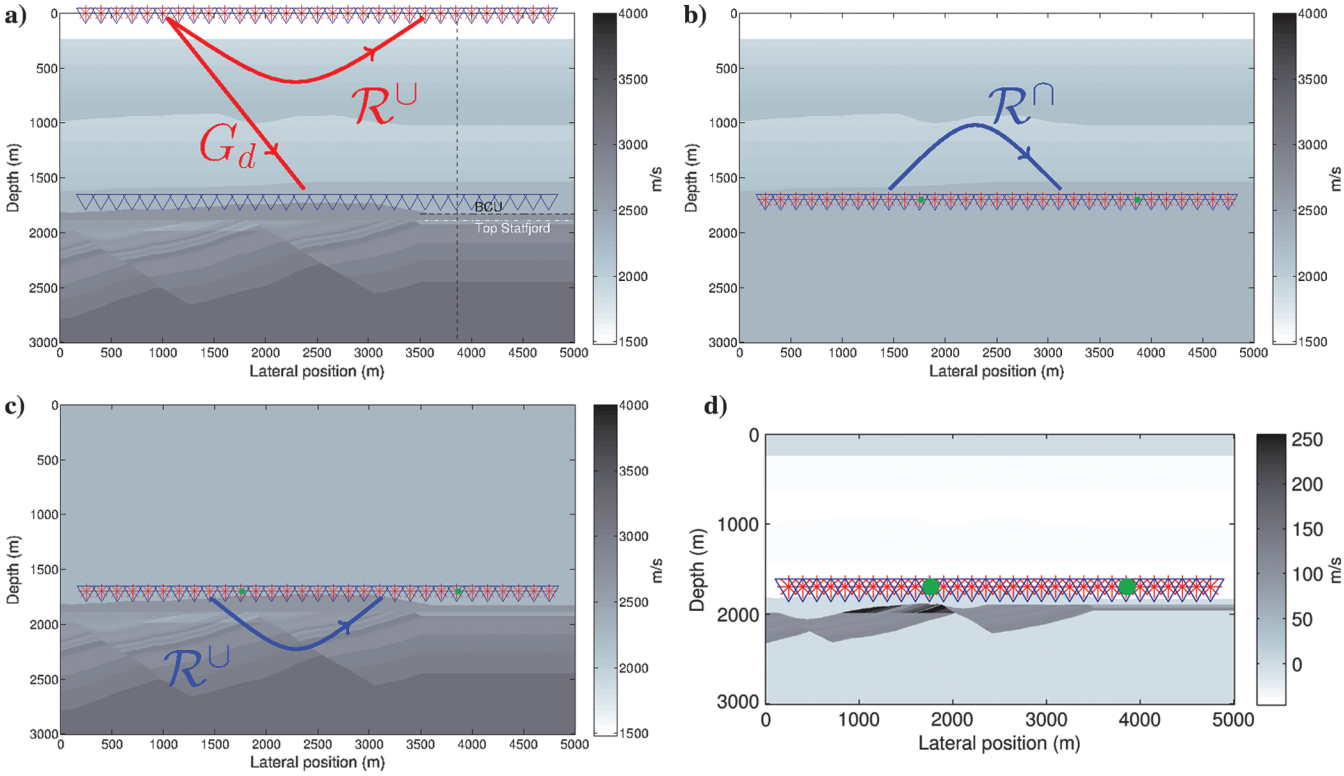

Figure 9. A P-wave velocity model of the Gullfaks field and the synthetic data sets geometries. The stars denote sources, and the triangles denote receivers. The red letters denote the input data, and the blue letters denote the unknown responses. (a) The base velocity model. The vertical dashed line indicates the position where the results are compared with that from the field data. Two major horizons below the borehole depth, namely, panel BCU and TS, are marked with horizontal dashed lines. (b) The medium configuration in which the responses of the overburden are retrieved. (c) The same as (b) but the underburden. (d) The overall velocity change. The green circles show the reference virtual source positions. The velocity changes are designed for comparison with the field measurement.

The base P-wave velocity model is shown in Figure 9a, in which the vertical dashed line ($x_1 = 3865$ m) indicates the reference position where the result will be compared with the field data. The velocity profile along this line is modified according to a well log. The two horizontal dashed lines mark the two horizons just below the synthetic well depth at 1700 m, namely, the Base Cretaceous Unconformity (BCU, 1830 m) and Top Statfjord (TS 1885 m). Figure 9b and 9c shows the medium states in which the new responses are retrieved. Figure 9d shows the overall time-lapse velocity change. The velocity change is zero in the layer below the BCU, and it is positive (100 m/s) in the layer below the TS due to the pore pressure drop (which is to be explained in the field data comparison subsection). The velocity change in the layers between the seabed and the BCU is made negative (2% decrease) to show that the detection of the velocity increase below the TS will not be affected using our method even when there is a velocity decrease above.

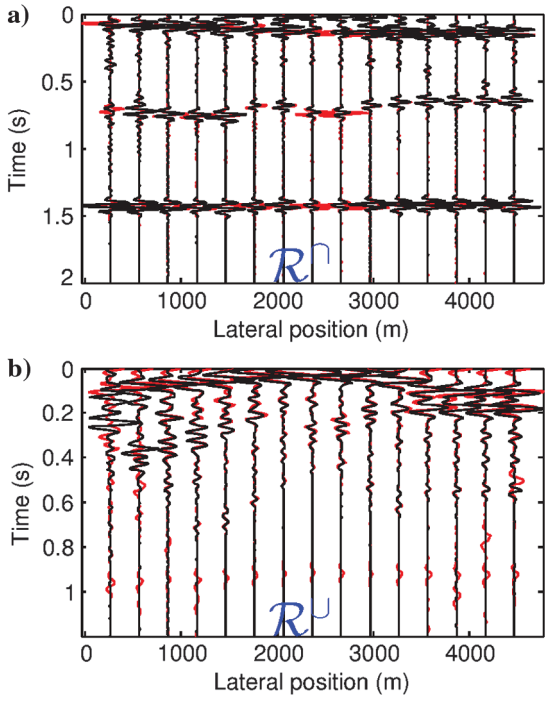

Figure 10. The validation of the new zero-offset responses in black against the modeled reference traces in red. The direct arrivals removed and the trace amplitude is normalized. The reflection response of (a) the overburden and (b) the underburden. The mismatch on both ends of the borehole in (b) is suspected to be due to the limited source aperture at the surface because the aperture is not much wider than the receiver apertures at the borehole depth. The limited receiver aperture could also be part of the reason because the integrals are truncated in solving equation 2. This aperture effect on the source side is less severe in (a) because of the two integral surface in equation 1 rather than one in equation 2.

For validation, Figure 10 shows the zero-offset comparison with the modeled responses (as in Figure 9b and 9c). The amplitudes are normalized, and the direct arrivals are removed. Figure 10a shows the reflection response of the overburden, and Figure 10b shows the reflection response of the underburden. The first observation is that all multiples from the other side are indeed removed as seen in the match of the late events. This gives an improved S/N for the events near the borehole, compared with the original data. Second, despite some mismatch, the phase of the reflections is overall well-recovered. The mismatches seen at the beginning and ending sides of the lateral position axis in Figure 10b are mainly due to the limited source aperture at the surface and the relatively large lateral inhomogeneity of the structures. For 4D applications, some of these phase mismatches between monitor and base surveys can be canceled out when traveltime differences are computed.

Next, for an overview of the new 4D responses, all zero-offset monitor traces are plotted in red over the base traces in black in Figure 11. In Figure 11b, the response of the underburden, the red signals (monitor response) arrive before those in black (base response) near the reservoir (close to the lateral position of 1500 m), and slightly after at the lateral position of 3865 m. This indicates a velocity increase in the reservoir and a slight decrease below the borehole near the lateral position of 3865 m. Such a subtle difference is not directly observable either in Figure 11c (the original surface data) or Figure 11d (the original borehole data). Moreover, identifying the reflections near the borehole in these data sets is difficult by itself due to multiple reflections and the ambiguity of direction of the reflections, whereas such problems are alleviated using this approach.

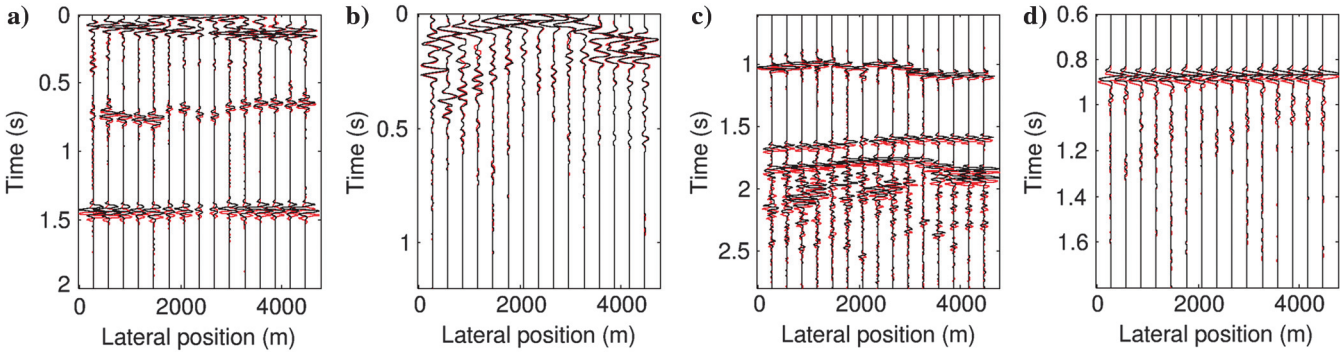

Figure 11. The overall zero-offset trace view of the base response (in black) and the monitor response (in red). The response of (a) the overburden and (b) the underburden. The increase in traveltime caused by the velocity decrease in the overburden is observable in (a), and so is the decrease in traveltime caused by the velocity increase in the underburden in (b). (c) A selected part of the original surface data with the direct arrivals removed. (d) A selected part of the borehole data with direct arrivals kept. Only positive time shifts are observable in (c and d). Because of the strong amplitude of the direct arrivals in (d), the identification of the reflections is not as clear as in (b).

For validation of the time shifts, detailed results for the lateral position of 1765 and 3865 m are shown in Figures 12 and 13, together with the velocity change profiles. The time shifts from the new responses are shown in blue, and those from the modeled responses are shown in red. The green line shows the time shift computed from the given velocities. The crosscorrelation window size is indicated in the figure captions. These two figures show that the time shifts are estimated correctly from the new responses and that the detailed small time shifts at each side of the borehole can be observed. Overall, the velocity increases below the borehole, but the velocity decreases slightly in the layer where the borehole is located, so a small positive time shift of approximately 1 ms is found in Figures 12d and 13d. For the area above the borehole, the velocity decrease in the model is also correctly matched by the positive time shifts in Figures 12b and 13b.

The overall time shift and time strain maps are shown in Figures 14 and 15, respectively, including those from the original surface and borehole data. Figure 14a shows the joined time shift map of the overburden and the underburden, separated by the dashed line as the borehole depth. Each half is calculated using the corresponding new responses shown in Figure 11a and 11b. Compared with Figure 14b and 14c from the original data, Figure 14a shows a correct separation of the time shifts above and below the borehole, and the changes in the deep part of the model are also present with correct positions. The change in the reservoir, marked by the circle, is clearly visible in Figure 14a. Note that no velocity information or primary picking is used during the process. Similarly, the joined time strain map in Figure 15a (the new responses) also shows more details than Figure 15b (the surface data) and 15c (the borehole data). Overall, it appears difficult to directly use the maps from the original data (Figures 14b, 14c, 15b, and 15c) for characterization near the borehole without any prior manual event interpretation.

Because this numerical experiment is designed for a comparison of the time shift of the event below TS to that from the field data, we end this section with a brief explanation on the field data.

The base data are acquired in one well, whereas water is being injected in another well, a few hundred meters away. Then, the monitor data are acquired after some waiting time. Figure 16 shows the two picked horizons (TS and BCU), in relation to the acquisition well position and some of the layer properties. From the field data, the average time shift for the event below TS is −0.7 ms (±0.5 ms). This corresponds to a velocity increase of approximately 40 m/s using the following relation (Landrø and Stammeijer, 2004), given a layer thickness of 60 m, zero layer thickness change, and a velocity of 2500 m/s in the layer,

$$\frac{\Delta t}{t} \approx \frac{\Delta z}{z} - \frac{\Delta v}{v}, \tag{10}$$

where t is the two-way time, z is the layer thickness, and v is the velocity of the layer.

In this model, the estimation of the layer thickness below TS (1885 m) ranges from 35 to 85 m. According to a time shift of −0.7 ms from the field data, this corresponds to a velocity increase of approximately 70 to 30 m/s. And for a time shift of 1.5 ms, the

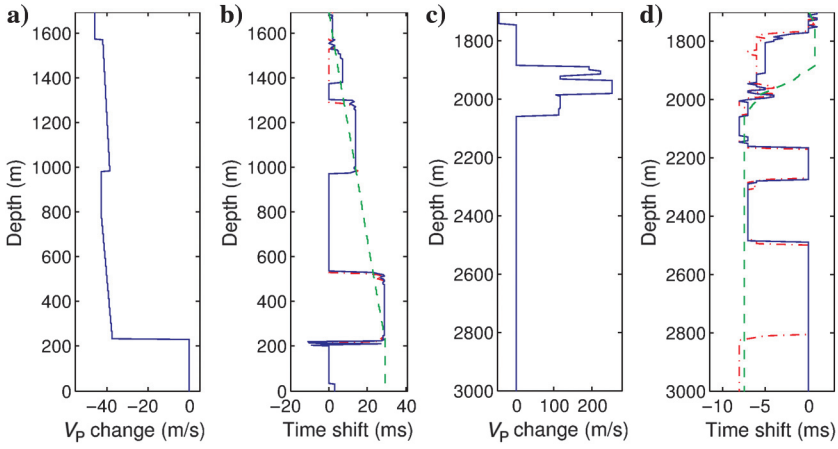

Figure 12. The velocity change profiles at $x_1 = 1765$ m of (a) the overburden and (c) the underburden. (b and d) The estimated time shifts from the new responses in Figure 11a and 11b, respectively. The blue line is obtained from the retrieved new response using cross correlation with a window size of 0.15 s for (a and b). The red dashed-dotted line is from the modeled response, and the green dashed line is computed directly from the velocities. The vertical axis in (a) is flipped to reflect that the retrieved response is obtained from below (see in Figure 9b). For a direct comparison, the results by crosscorrelation are converted to depth using the base velocities. Some of the time shifts by crosscorrelation go to zero because the amplitudes of late events are small and a threshold value for crosscorrelation is used for stability.

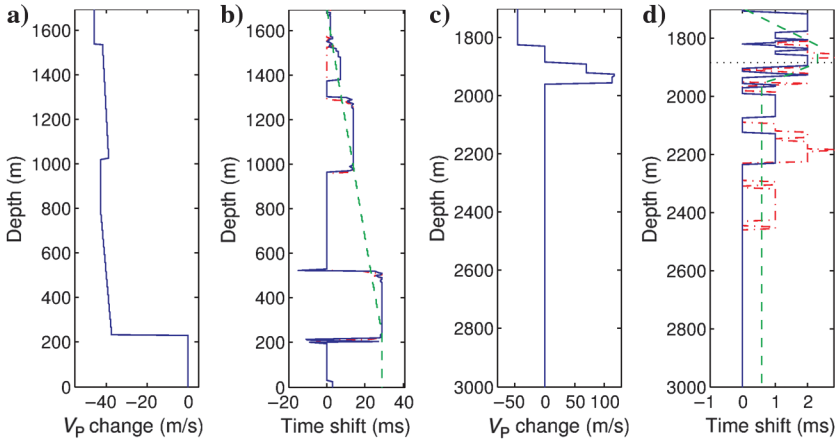

Figure 13. The velocity change profiles at $x_1 = 3865$ m of (a) the overburden and (c) the underburden. (b and d) The estimated time shifts from the new responses in Figure 11a and 11b, respectively. The blue line is obtained from the retrieved new response using crosscorrelation with a window size of 0.15 s for (a) and 0.1 s for (b). The red dashed-dotted line is calculated from the modeled response, and the green dashed line is computed directly from the velocities. The black dotted line in (d) indicates the layer below the TS (1885 m).

corresponding velocity change is approximately 130 and 60 m/s. Therefore, in the numerical modeling, a velocity increase of 70 m/s is used (Figure 13c), so a time shift of approximately −1 ms should be expected.

Another comment regarding the synthetic monitor velocity model is that a velocity decrease above BCU is used, which is not likely the case for the field data. But this velocity decrease is used here to show that one can estimate the traveltime change in the underburden, without any effect from the overburden. And likewise, one can estimate the traveltime change in the overburden, without any effect from the underburden.

Figure 17 shows the detailed time shift from the new response at $x = 3865$ m. For a comparison with the field data result that is targeted to the event below the TS, one should first take the difference of the time shift at the TS and the layer below. As indicated in the figure, the difference is estimated to be −1 ms; therefore, this is in reasonable agreement with the expected value and the field data observation of −0.7 ms.

DISCUSSION

The proposed method aims at separating the reflection responses above and below a horizontal borehole without any velocity information. Based on the two numerical examples, we see that the method is good at detecting small changes (<1 ms) near the borehole. This sensitivity to small velocity change has similarly been observed in coda wave interferometry; this is because parts of the coda are preserved in the retrieved responses. But different from conventional coda wave interferometry, there is also a separation of the coda above and below the borehole (for this scenario) because the full waveforms are retrieved in truncated media.

For the 2D case with a horizontal borehole, the examples show that this approach is useful for time-lapse characterization of the deep part of the model, even for small velocity changes. Correct and detailed time shifts directly related to changes near the borehole are found. The process is completely data driven in this 2D case, and no velocity information is needed. The use of borehole data has significant benefits, especially for time-lapse studies (Bakulin et al., 2007) because the measured data in boreholes naturally account for the changes in the overburden. In case the measured direct arrival is

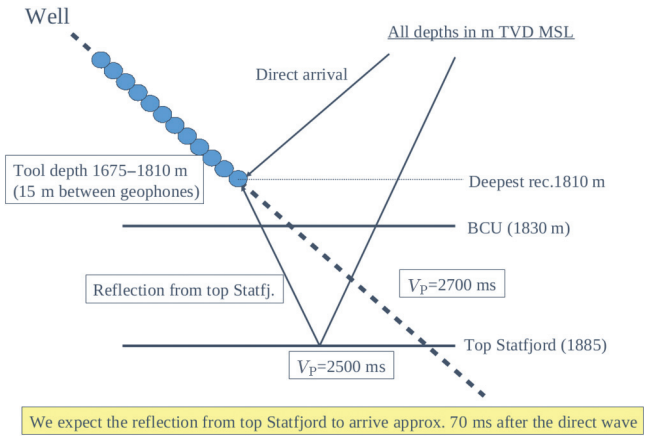

Figure 16. A sketch of the major horizons in relation to the acquisition well.

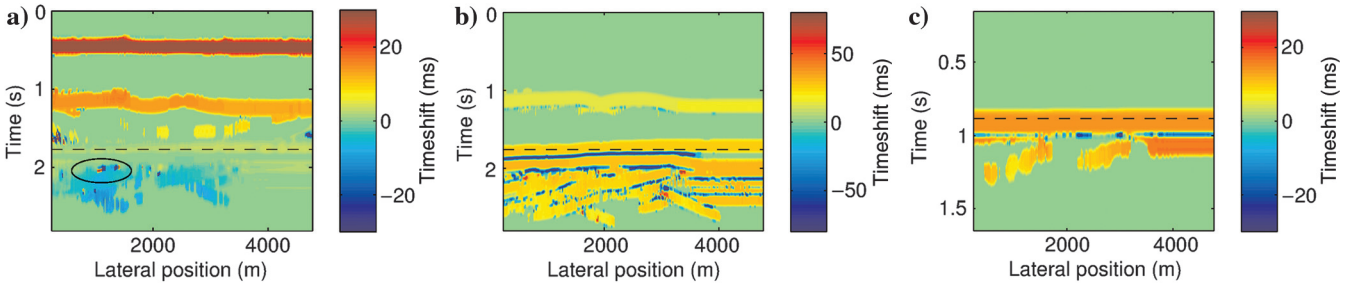

Figure 14. The smoothed time shift maps as in Figure 7. (a) The joined map of the overburden and the underburden. (b and c) The individual maps from the original surface reflection and the borehole data, respectively. The dashed line indicates the borehole depth in time. The cross-correlation window is 0.15 s for all panels. The circled area indicates the location of the changes in the reservoir.

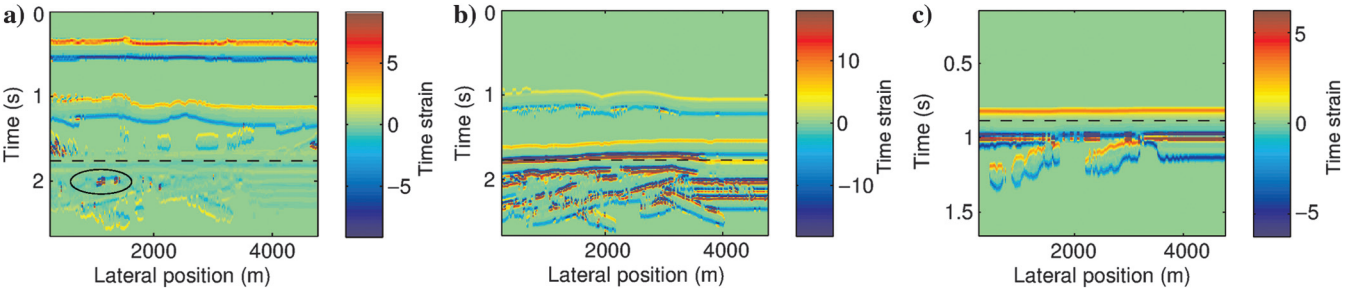

Figure 15. The time strain maps based on Figure 14. The joined map in (a) shows correctly the position of the changes in the model, whereas these features are lacking in the maps from the original surface data in (b) and borehole data in (c). The change in the reservoir is highlighted by the eclipse.

not satisfactory, some interpolation based on the existing traveltime curve can be used without using a velocity model. Furthermore, in case the focusing function cannot be found, approximate solutions (Liu et al., 2016) to the desired reflection responses are still sufficient for evaluating the changes close to the borehole, except that the multiples are not completely removed in that case. The added advantage of using the Marchenko scheme allows the retrieval of the reflection response using single-component data without any multiples from the other side of the borehole. Some small reflection events that are difficult to identify from the original surface or borehole data can be retrieved automatically by this method.

This method provides a different way of using the borehole data, complementing well with those that use the direct arrivals for the changes at shallower depths (Zadeh and Landrø, 2011). Regarding the amplitude and amplitude variation with offset inversion studies, we believe it is possible to use the relative amplitudes of the new response, provided that a wide survey aperture is available at the surface and the survey repeatability issue is manageable.

For a 3D application, if there is an adequate coverage with multiple horizontal boreholes, the method can be still be described as velocity independent. But a more realistic case would be that there is only partial coverage with horizontal boreholes. Then, the direct arrivals from a single borehole would not be enough to describe the traveltime from the target plane to the surface. Local interpolation near the well should be considered, and velocity information would be needed in that case, but only for the volume between the borehole level to the surface. Therefore, for the use of existing velocity models, it would most likely be necessary for 3D application. Then, in the case of an erroneous velocity model, ghost events are observed in the up-down wavefields (Thorbecke et al., 2013) when there are phase errors in direct arrivals, whereas the amplitude errors may be corrected (de Ridder et al., 2016).

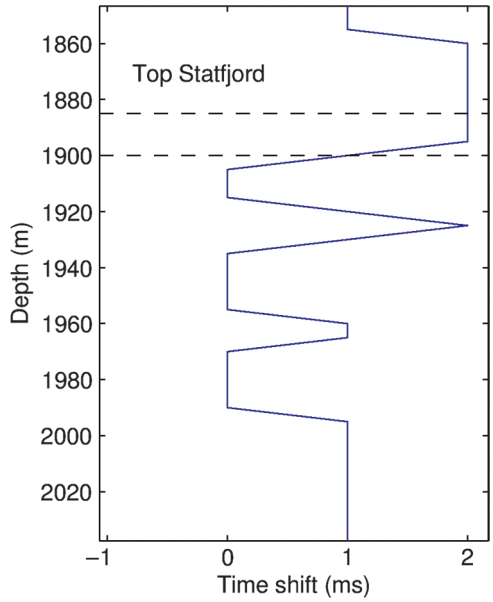

Figure 17. The detailed time shift from Figure 13d for comparison with the field data result. The upper dashed black line denotes the depth of the TS, and the lower line denotes the depth of 1900 m. The time shift decreases from 2 ms at the TS to 1 ms at the second line. This corresponds to a time shift of −1 ms for this layer. The average time shift from the field data for the event below the TS is −0.7 ms.

Other concerning practical issues are the following: A wide source coverage at the surface is desirable for retrieving the correct phase and amplitude information in the new responses. The source signal deconvolution and free-surface multiple removal are assumed in the numerical examples, but they should be dealt with in practice. In addition, we assume a lossless medium in modeling the data. For the latter two, the extension to include surface-related multiples in the Marchenko method is shown by Singh et al. (2017) and the Marchenko method for dissipative media is discussed by Slob et al. (2016).

Regarding nonhorizontal boreholes, if the well is only slightly deviated, then one could first apply some local phase shift to adjust the borehole data to a desired level before using the method. That would require the velocity of that level only, not a complete velocity model. On the other hand, the restriction to horizontal boreholes is lifted when a good background velocity model is available. Because the full Marchenko method can provide the focusing functions and up-down wavefield at every grid point in the model, numerous possibilities for modeling, imaging, and monitoring open up (Wapenaar et al., 2014; Meles et al., 2016; van der Neut and Wapenaar, 2016).

CONCLUSION

We present a new approach to combine data at the surface and in a horizontal borehole for finding the traveltime changes close to the borehole. The numerical examples show that the time shifts for the deep events are obtained correctly without any manual event picking. The location and the magnitude of the changes near the borehole are identified more clearly than those from the original data. For 2D, the method is completely data driven given a good source coverage at the surface. For 3D, it is most likely that interpolation for the direct traveltime is needed. Although practical limitations related to the Marchenko method exist, we believe that this proposal of joining the surface data with the borehole data is nevertheless worth exploiting for robust subsurface monitoring.

ACKNOWLEDGMENTS

The authors acknowledge the Norwegian Research Council and the sponsors of the ROSE consortium at NTNU for financial support, and J. Thorbecke at TU Delft for the open source modeling package. The authors thank the associate editor and the reviewers for their comments that helped to improve the paper.

REFERENCES

Amundsen, L., 2001, Elimination of free-surface related multiples without need of the source wavelet: Geophysics, **66**, 327–341, doi: 10.1190/1.1444912.

Bakulin, A., and R. Calvert, 2006, The virtual source method: Theory and case study: Geophysics, **71**, no. 4, SI139–SI150, doi: 10.1190/1.2216190.

Bakulin, A., A. Mateeva, K. Mehta, P. Jorgensen, J. Ferrandis, I. Sinha Herhold, and J. Lopez, 2007, Virtual source applications to imaging and reservoir monitoring: The Leading Edge, **26**, 732–740, doi: 10.1190/1.2748490.

Barkved, O. I., and T. Kristiansen, 2005, Seismic time-lapse effects and stress changes: Examples from a compacting reservoir: The Leading Edge, **24**, 1244–1248, doi: 10.1190/1.2149636.

Behura, J., K. Wapenaar, and R. Snieder, 2014, Autofocus imaging: Image reconstruction based on inverse scattering theory: Geophysics, **79**, no. 3, A19–A26, doi: 10.1190/geo2013-0398.1.

Broggini, F., R. Snieder, and K. Wapenaar, 2012, Focusing the wavefield inside an unknown 1D medium: Beyond seismic interferometry: Geophysics, **77**, no. 5, A25–A28, doi: 10.1190/geo2012-0060.1.

de Ridder, S., A. Curtis, J. van der Neut, and K. Wapenaar, 2016, Marchenko wavefield redatuming, imaging conditions, and the effect of model errors: 86th Annual International Meeting, SEG, Expanded Abstracts, 5155–5159, doi: 10.1190/segam2016-13777555.1.

Fuck, R. F., A. Bakulin, and I. Tsvankin, 2009, Theory of traveltime shifts around compacting reservoirs: 3D solutions for heterogeneous anisotropic media: Geophysics, **74**, no. 1, D25–D36, doi: 10.1190/1.3033215.

Galetti, E., and A. Curtis, 2012, Generalised receiver functions and seismic interferometry: Tectonophysics, **532–535**, 1–26, doi: 10.1016/j.tecto.2011.12.004.

Guilbot, J., and B. Smith, 2002, 4-D constrained depth conversion for reservoir compaction estimation: Application to Ekofisk Field: The Leading Edge, **21**, 302–308, doi: 10.1190/1.1463782.

Guitton, A., and D. J. Verschuur, 2004, Adaptive subtraction of multiples using the L1-norm: Geophysical Prospecting, **52**, 27–38, doi: 10.1046/j.1365-2478.2004.00401.x.

Hatchell, P., and S. Bourne, 2005, Rocks under strain: Strain-induced time-lapse time shifts are observed for depleting reservoirs: The Leading Edge, **24**, 1222–1225, doi: 10.1190/1.2149624.

Hodgson, N., C. MacBeth, L. Duranti, J. Rickett, and K. Nihei, 2007, Inverting for reservoir pressure change using time-lapse time strain: Application to genesis field, Gulf of Mexico: The Leading Edge, **26**, 649–652, doi: 10.1190/1.2737104.

Landrø, M., P. Digranes, and L. K. Strønen, 2001, Technical article: Mapping reservoir pressure and saturation changes using seismic methods — Possibilities and limitations: First Break, **19**, 671–684, doi: 10.1046/j.1365-2397.2001.00226.x.

Landrø, M., O. A. Solheim, E. Hilde, B. O. Ekren, and L. K. Strønen, 1999, The Gullfaks 4D seismic study: Petroleum Geoscience, **5**, 213–226, doi: 10.1144/petgeo.5.3.213.

Landrø, M., and J. Stammeijer, 2004, Quantitative estimation of compaction and velocity changes using 4D impedance and traveltime changes: Geophysics, **69**, 949–957, doi: 10.1190/1.1778238.

Liu, Y., J. van der Neut, B. Arntsen, and K. Wapenaar, 2016, Combination of surface and borehole seismic data for robust target-oriented imaging: Geophysical Journal International, **205**, 758–775, doi: 10.1093/gji/ggw011.

Maharramov, M., B. Biondi, and M. Meadows, 2015, Simultaneous TV-regularized time-lapse FWI with application to field data: 85th Annual International Meeting, SEG, Expanded Abstracts, 1236–1241, doi: 10.1190/segam2015-5925444.1.

Maharramov, M., B. L. Biondi, and M. A. Meadows, 2016, Time-lapse inverse theory with applications: Geophysics, **81**, no. 6, R485–R501, doi: 10.1190/geo2016-0131.1.

Mehta, K., J. Sheiman, R. Snieder, and R. Calvert, 2008, Strengthening the virtual-source method for time-lapse monitoring: Geophysics, **73**, no. 3, S73–S80, doi: 10.1190/1.2894468.

Meles, G. A., K. Löer, M. Ravasi, A. Curtis, and C. A. da Costa Filho, 2015, Internal multiple prediction and removal using Marchenko autofocusing and seismic interferometry: Geophysics, **80**, no. 1, A7–A11, doi: 10.1190/geo2014-0408.1.

Meles, G. A., K. Wapenaar, and A. Curtis, 2016, Reconstructing the primary reflections in seismic data by Marchenko redatuming and convolutional interferometry: Geophysics, **81**, no. 2, Q15–Q26, doi: 10.1190/geo2015-0377.1.

Menke, W., 1989, Geophysical data analysis: Discrete inverse theory: Academic Press.

Meunier, J., and F. Huguet, 1998, Cere-la-Ronde; a laboratory for time-lapse seismic monitoring in the Paris Basin: The Leading Edge, **17**, 1388–1394, doi: 10.1190/1.1437856.

Meunier, J., F. Huguet, and P. Meynier, 2001, Reservoir monitoring using permanent sources and vertical receiver antennae: The Cere-la-Ronde case study: The Leading Edge, **20**, 622–629, doi: 10.1190/1.1439008.

Raknes, E. B., and B. Arntsen, 2014, Time-lapse full-waveform inversion of limited-offset seismic data using a local migration regularization: Geophysics, **79**, no. 3, WA117–WA128, doi: 10.1190/geo2013-0369.1.

Ravasi, M., I. Vasconcelos, A. Kritski, A. Curtis, C. Alberto da Costa Filho, and G. A. Meles, 2016, Target-oriented Marchenko imaging of a North Sea field: Geophysical Journal International, **205**, 99–104, doi: 10.1093/gji/ggv528.

Rickett, J., L. Duranti, T. Hudson, B. Regel, and N. Hodgson, 2007, 4d time strain and the seismic signature of geomechanical compaction at genesis: The Leading Edge, **26**, 644–647, doi: 10.1190/1.2737103.

Røste, T., O. P. Dybvik, and O. K. Sreide, 2015, Overburden 4d time shifts induced by reservoir compaction at snorre field: The Leading Edge, **34**, 1366–1374, doi: 10.1190/tle34111366.1.

Røste, T., M. Landrø, and P. Hatchell, 2007, Monitoring overburden layer changes and fault movements from time-lapse seismic data on the Valhall field: Geophysical Journal International, **170**, 1100–1118, doi: 10.1111/j.1365-246X.2007.03369.

Singh, S., R. Snieder, J. van der Neut, J. Thorbecke, E. Slob, and K. Wapenaar, 2017, Accounting for free-surface multiples in Marchenko imaging: Geophysics, **82**, no. 1, R19–R30, doi: 10.1190/geo2015-0646.1.

Slob, E., C. Wapenaar, and J. Thorbecke, 2016, Marchenko equations for acoustic Green's function retrieval and imaging in dissipative media: 86th Annual International Meeting, SEG, Expanded Abstracts, 5160–5165, doi: 10.1190/segam2016-13788610.1.

Snieder, R., M. Miyazawa, E. Slob, I. Vasconcelos, and K. Wapenaar, 2009, A comparison of strategies for seismic interferometry: Surveys in Geophysics, **30**, 503–523, doi: 10.1007/s10712-009-9069-z.

Thorbecke, J., and D. Draganov, 2011, Finite-difference modeling experiments for seismic interferometry: Geophysics, **76**, no. 6, H1–H18, doi: 10.1190/geo2010-0039.1.

Thorbecke, J., J. van der Neut, and K. Wapenaar, 2013, Green's function retrieval with Marchenko equations: A sensitivity analysis: 83rd Annual International Meeting, SEG, Expanded Abstracts, 3888–3893, doi: 10.1190/segam2013-1034.1.

van der Neut, J., and K. Wapenaar, 2016, Adaptive overburden elimination with the multidimensional marchenko equation: Geophysics, **81**, no. 5, T265–T284, doi: 10.1190/geo2016-0024.1.

Wapenaar, K., F. Broggini, E. Slob, and R. Snieder, 2013, Three-dimensional single-sided Marchenko inverse scattering, data-driven focusing, Green's function retrieval, and their mutual relations: Physical Review Letters, **110**, 084301, doi: 10.1103/PhysRevLett.110.084301.

Wapenaar, K., J. Thorbecke, J. van der Neut, F. Broggini, E. Slob, and R. Snieder, 2014, Marchenko imaging: Geophysics, **79**, no. 3, WA39–WA57, doi: 10.1190/geo2013-0302.1.

Wapenaar, K., J. van der Neut, E. Ruigrok, D. Draganov, J. Hunziker, E. Slob, J. Thorbecke, and R. Snieder, 2011, Seismic interferometry by crosscorrelation and by multidimensional deconvolution: A systematic comparison: Geophysical Journal International, **185**, 1335–1364, doi: 10.1111/j.1365-246X.2011.05007.

Wapenaar, K., J. van der Neut, and E. Slob, 2016, Unified double- and single-sided homogeneous Green's function representation: Proceedings of the Royal Society A, **472**, 20160162, doi: 10.1098/rspa.2016.0162.

Whitcombe, D. N., P. Paramo, N. Philip, A. Toomey, T. Redshaw, and S. Linn, 2010, The correlated leakage method — Its application to better quantify timing shifts on 4D data: 72nd Annual International Conference and Exhibition, EAGE, Extended Abstracts, B037.

Zadeh, M. H., and M. Landrø, 2011, Monitoring a shallow subsurface gas flow by time lapse refraction analysis: Geophysics, **76**, no. 6, O35–O43, doi: 10.1190/geo2011-0012.1.